



OPEN

Atomically resolved spectroscopic study of Sr_2IrO_4 : Experiment and theory

SUBJECT AREAS:

PHASE TRANSITIONS
AND CRITICAL
PHENOMENAELECTRONIC PROPERTIES AND
MATERIALS

ELECTRONIC STRUCTURE

SURFACES, INTERFACES AND
THIN FILMSReceived
11 April 2013Accepted
11 October 2013Published
29 October 2013

Correspondence and requests for materials should be addressed to M.H.P. (panm@ornl.gov) or D.G.M. (dmandrus@utk.edu)

* These authors contributed equally to this work.

Qing Li^{1,9*}, Guixin Cao^{2,3*}, Satoshi Okamoto³, Jieyu Yi^{2,3}, Wenzhi Lin¹, Brian C. Sales³, Jiaqiang Yan^{2,3}, Ryotaro Arita^{4,5}, Jan Kuneš⁶, Anton V. Kozhevnikov⁷, Adolfo G. Eguiluz⁸, Masatoshi Imada^{4,5}, Zheng Gai¹, Minghu Pan¹ & David G. Mandrus^{2,3}

¹Center for Nanophase Materials Sciences, Oak Ridge National Laboratory, Oak Ridge, TN 37831, USA, ²Department of Materials Science and Engineering, University of Tennessee, Knoxville, TN 37996, USA, ³Materials Science and Technology Division, Oak Ridge National Laboratory, Oak Ridge, TN 37831, USA, ⁴Department of Applied Physics, University of Tokyo, Hongo, Bunkyo-ku, Tokyo, 113-8656, Japan, ⁵JST-CREST, Hongo, Bunkyo-ku, Tokyo, 113-8656, Japan, ⁶Institute of Physics, Academy of Sciences of the Czech Republic, Cukrovarnická 10, Praha 6, 162 53, Czech Republic, ⁷Institute for Theoretical Physics, ETH Zurich, CH-8093 Zurich, Switzerland, ⁸Department of Physics and Astronomy, University of Tennessee, Knoxville, 37996, USA, ⁹Institute of Functional Nano & Soft Materials (FUNSOM), Soochow University, Suzhou, Jiangsu 215123, China.

Particularly in Sr_2IrO_4 , the interplay between spin-orbit coupling, bandwidth and on-site Coulomb repulsion stabilizes a $J_{\text{eff}} = 1/2$ spin-orbital entangled insulating state at low temperatures. Whether this insulating phase is Mott- or Slater-type, has been under intense debate. We address this issue via spatially resolved imaging and spectroscopic studies of the Sr_2IrO_4 surface using scanning tunneling microscopy/spectroscopy (STM/S). STS results clearly illustrate the opening of an insulating gap (150 ~ 250 meV) below the Néel temperature (T_N), in qualitative agreement with our density-functional theory (DFT) calculations. More importantly, the temperature dependence of the gap is qualitatively consistent with our DFT + dynamical mean field theory (DMFT) results, both showing a continuous transition from a gapped insulating ground state to a non-gap phase as temperatures approach T_N . These results indicate a significant Slater character of gap formation, thus suggesting that Sr_2IrO_4 is a uniquely correlated system, where Slater and Mott-Hubbard-type behaviors coexist.

In 3d transition metal oxides (TMOs), the localized 3d states are responsible for the narrow 3d bandwidth (W) and the accompanying strong on-site Coulomb repulsion (U). By contrast, in 5d correlated electronic systems, the strong spin-orbit coupling (SOC) is comparable to W and U . The interplay between U , W and SOC gives rise to a broad spectrum of novel phenomena, e. g. the metal-insulator transition (MIT) may switch from Mott type to Slater type¹.

Recently, intensive studies have been carried out on the layered 5d TMO, Sr_2IrO_4 , owing to the structural and electronic similarities to parent high- T_c cuprates, such as La_2CuO_4 . It has been established that Sr_2IrO_4 exhibits insulating behavior^{2,3}, with predominant antiferromagnetic (AFM) order developing below the Néel temperature (T_N) (~240 K)⁴. Based on the calculated band structure, Kim *et al.*⁵ proposed that Sr_2IrO_4 is a canted AF Mott insulator. In this scenario the interplay between SOC, W and U stabilizes a novel ground state electronic structure of Sr_2IrO_4 , consisting of completely filled $J_{\text{eff}} = 3/2$ bands and a narrow half-filled $J_{\text{eff}} = 1/2$ band near the Fermi level (E_F). The $J_{\text{eff}} = 1/2$ band is split into an upper Hubbard band (UHB) and lower Hubbard band (LHB) by moderate Coulomb repulsion⁶, exhibiting antiferromagnetic ordering of the effective $J_{\text{eff}} = 1/2$ moments. Such a $J_{\text{eff}} = 1/2$ Mott-Hubbard scenario has been suggested from ARPES⁷ and RXS⁵ measurements. However, several recent papers challenge this strong spin-orbit interaction (SOI) limit $J_{\text{eff}} = 1/2$ ground-state scenario. For example, X-ray absorption⁸ studies of Sr_2IrO_4 found that magnetic exchange (~200 meV) and tetragonal crystal field (~75 meV) interactions modify the electronic ground state away from the strong SOI limit $J_{\text{eff}} = 1/2$ state, suggesting that the magnetic transition has implications for the origin of the insulating gap. Also, time-resolved optical studies⁹ found that upon cooling through T_N the system evolves continuously from a metal-like phase to a gapped phase, the hallmark of a Slater MIT. A very recent neutron diffraction investigation¹⁰ of single-crystal Sr_2IrO_4 found that the system undergoes an antiferromagnetic transition with an ordered moment of 0.208 μ_B per Ir site. This measured magnetic moment is much smaller than 1 μ_B , conventionally anticipated for an $S = 1/2$ system, strongly challenging the scenario that Sr_2IrO_4 is a strongly correlated Mott insulator with the $J_{\text{eff}} = 1/2$



ground-state expected from the simple SOI limit. All these reported results suggest that the $J_{\text{eff}} = 1/2$ Mott-Hubbard scenario may be not the sole mechanism for explaining this unique, $5d$ correlated material.

Indeed, Arita *et al.* have proposed a Slater mechanism for the gap formation in Sr_2IrO_4 ¹¹. Such a Slater mechanism has been found in other $5d$ TMOs such as NaOsO_3 ¹², where the Slater transition is demonstrated unambiguously by showing the coincidence of MIT and the onset of long-range commensurate magnetic order based on the results of neutron and X-ray scattering. The role of magnetic interactions in gap formation has remained a matter of debate with Sr_2IrO_4 alternatively labeled a Mott-Hubbard insulator (Coulomb and exchange interactions drive gap formation), Mott insulator (Coulomb interactions alone drive gap formation) and more recently a Slater insulator (magnetic ordering drives gap formation).

In this article, we determine the atomically-resolved surface structure of Sr_2IrO_4 using scanning tunneling microscopy/spectroscopy (STM/S) and low-energy electron diffraction (LEED). Clear evidence from tunneling spectra shows a continuous evolution of the insulating gap as the sample is cooled below the magnetic transition. This is strong evidence that the insulating gap and magnetic order are correlated, which is a signature of Slater-type gap formation. Some of the tunneling spectra display a build-up of states at the gap edges, in remarkable qualitative agreement with our first principles dynamical mean field theory calculations. We conclude that although Sr_2IrO_4 is clearly not a simple, weak-coupling Slater insulator, gap formation in this system is strongly tied to magnetic order and displays a strong Slater character.

Results

Sr_2IrO_4 crystallizes in the layered perovskite K_2NiF_4 structure and has octahedrally coordinated Ir^+ ions as shown in Fig. 1a⁴. Details of crystal growth and basic characterization are described in the Materials and Methods section. For the STM/S measurements,

Sr_2IrO_4 single crystals were cleaved *in situ* in an ultra-high vacuum environment at room temperature, producing a mirror-like surface. From crystal-chemical considerations and experience with other layered perovskites such as Sr_2RuO_4 ^{13–15}, the cleavage occurs between the Sr-O planes (see Fig. 1a) and exposes the (001) surface. After cleavage, and without breaking vacuum, the crystal was immediately mounted into the cryogenic STM. To minimize thermal drift, both the sample and STM were cooled simultaneously. Figure 1b shows a $200 \times 200 \text{ nm}^2$ topographic image of a cleaved Sr_2IrO_4 surface measured at 80 K in constant current mode. The height of a step is 12.8 \AA , in good agreement with the single step height of the (001) terminated surface. A “square-like” lattice is barely visible in Fig. 1c, the zoom-in area denoted in Fig. 1b by a white square, with an in-plane lattice constant of 3.8 \AA , which reflects a termination of primary 1×1 structure truncated from a tetragonal bulk crystal (see Fig. 1a).

A typical LEED image at room temperature is shown in Fig. 1d. The unit cell derived from the LEED pattern appears to reflect a 1×1 surface expected for an $I4/mmm$ tetragonal structure and consistent with STM observations. In addition to the 1×1 pattern, additional spots are also clearly revealed, implying a $\sqrt{2} \times \sqrt{2}$ enlarged unit cell. Such $\sqrt{2} \times \sqrt{2}$ cells have been observed on other TMO surfaces such as Sr_2RuO_4 and $\text{Sr}_3\text{Ru}_2\text{O}_7$ ^{14,16} and are due to rotations of the MO_6 octahedra. In Sr_2IrO_4 neutron diffraction measurements found the IrO_6 octahedra in Sr_2IrO_4 compound are indeed rotated around the crystallographic c axis by about 11° , thus reducing the space group symmetry from $I4/mmm$ to $I4_1/acd$ and generating an enlarged unit cell with dimensions $\sqrt{2}a \times 2c$ ⁴. Temperature-dependent LEED measurements (Fig. S1) show no structural change occurs on the (001) surface from room temperature to 150 K, ruling out a structural transition on the surface.

In contrast to its $4d$ counterpart Sr_2RhO_4 , a 2D Fermi liquid, Sr_2IrO_4 is unexpectedly a canted antiferromagnetic insulator^{4,10,17}. Magnetization measurements display weak ferromagnetism below

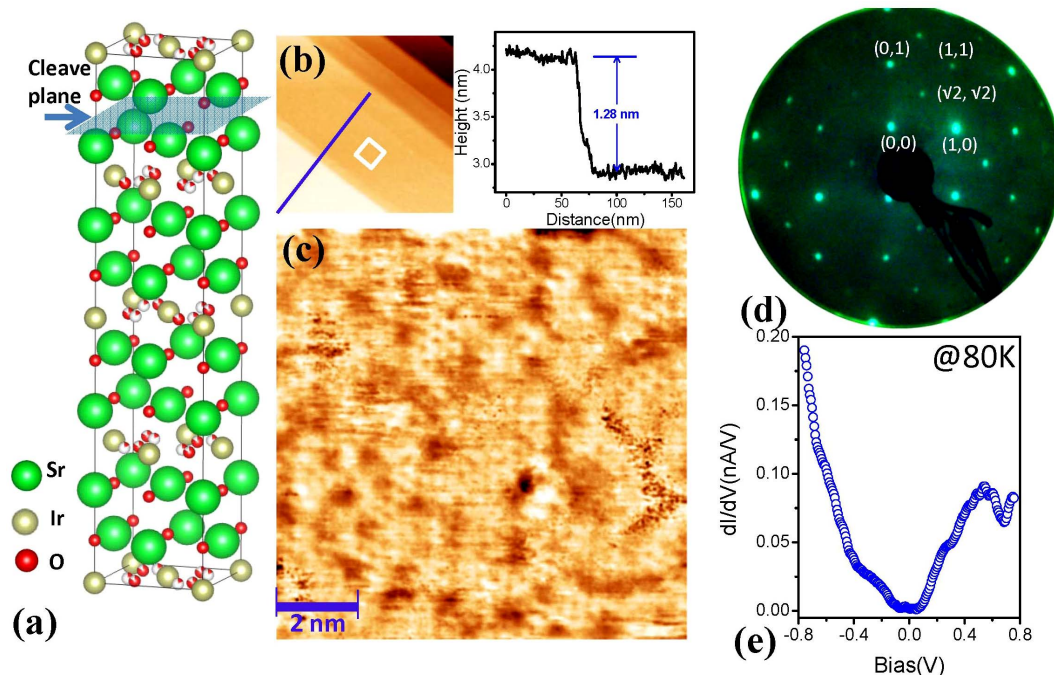


Figure 1 | Characterization of (001) cleaved Sr_2IrO_4 surface. (a), A ball model of the crystal structure of Sr_2IrO_4 . (b), A typical topographic image of the (001) surface. The setup conditions for imaging were a sample-bias voltage of 50 mV and a tunneling current of 0.1 nA. The surface was created by cleavage between two SrO layers without breaking IrO_6 octahedra. The right panel shows a cross-section along the line in the left panel. (c), Atomically resolved image shows a square lattice of Sr atoms. (d), A typical LEED image at the cleaved (001) surfaces of Sr_2IrO_4 measured at room temperature. LEED pattern shows 1×1 and $\sqrt{2} \times \sqrt{2}$ fractional spots (marked by arrows). (e), Averaged tunneling spectrum taken at 80 K, showing the opening insulating gap (averaged over an area of $100 \text{ nm} \times 100 \text{ nm}$ by a grid spectroscopic mode with 20×20 sampling pixels). Data were taken with a sample bias voltage of -50 mV and a tunneling current of 0.1 nA. Bias-modulation amplitude was set to $3 \text{ mV}_{\text{rms}}$.



240 K with an easy axis along the a -axis¹⁷, which agree with our electrical resistivity and magnetic measurements.

Scanning Tunneling Spectroscopy (STS) probes the integrated surface density of electronic states (DOS) by measuring the tunneling conductance (the derivative of the tunneling current, dI/dV). Averaged STS spectra obtained at 80 K are shown in Fig. 1e; an insulating gap with width of approximately 0.20 eV is readily apparent. The blurring of gap structure is mainly due to the gap geometry in k -space. The gap symmetry can be investigated by tunneling into an arbitrary plane differing from (001). The DOS measured by an STS is simply an average over k -space. Most published STM experiments on cleaved oxides have been carried out with the STM tip positioned perpendicular, c -axis tunneling, to the (001) surface, resulting in an angular average over the ab -plane density of states^{18,19}. There have been few attempts to perform cross-sectional tunneling^{20–23}, *i.e.*, tunneling into an arbitrary plane parallel to the [001] direction, particularly attractive for high- T_c cuprates. Cross-sectional tunneling is a challenging endeavor, which becomes even harder for atomically resolved cross-section imaging^{24,25}, primarily due to the difficulty in preparing a suitable cross-section for STM. Cleaving along other planes (instead of the (001) surface) is very unlikely because of the strong bonding between the metal ion and oxygen. In Sr_2IrO_4 , however, we occasionally observe some high-index facets in our STM images after cleaving. STM/S measurements of the gap structure on these exposed facets, due to a different average over k , yielded a well-developed gap structure and allowed us to better quantify the evolution of the gap with temperature.

Figure 2a shows a three dimensional, topographic STM image. Two crystallographic planes with different orientations are visible in this image. The surface in upper left corner is the normal (001) plane, which was the most frequently observed surface in our STM imaging. After carefully comparing against the crystal structure of Sr_2IrO_4 , we were able to assign the facet in right corner to the (661) plane (see supporting materials Fig. S2 for details).

The atomic structures for the two orientated surfaces, (001) and (661), are shown in Fig. 2b, which exhibit a Sr-comprised square and a mixed Sr-Ir near-hexagonal lattice, respectively. Tunneling spectra at 4.2 K (Fig. 2c) exhibits similar gap size but with different gap features at the two orientated surfaces. The gap on (001) surface is shallow with indistinct gap edges (blue (color) curve in the upper panel). However, the gap observed on the (661) facet is sharper with better-defined edges (red (color) curve in the bottom panel) compared to (001) surface. Such different gap features observed at two orientated surfaces suggest anisotropic gap geometry in k -space. In analogy to a d -wave superconductor, the insulating gap in Sr_2IrO_4 is angle-dependent. With different tunneling configurations, the DOS measured by STS are a different average over k -space, therefore producing different gap features. From the fitting of the gap feature on (661) surface, we derive the gap size about 164 meV measured at 4.2 K, indicating an insulating phase at low temperature. The gap of Sr_2IrO_4 has been reported with diverse values from 0.1 eV to 0.4 eV³ based on various measurements. It is worth noting that the insulating gap of the bulk Sr_2IrO_4 is reported consistently to be around 0.1 eV or less^{7,26}, smaller than our observed value on the surface. This fact is consistent with the conventional picture that electron-electron correlation effects should be stronger at the surface than that in the bulk as a result of the reduced atomic coordination¹⁵. We noticed two STM works recently posted in the *archive* by Nichols *et al.*²⁷ and Dai *et al.*²⁸, which reported the observation of an unusually large gap with the size up to 620 meV on Sr_2IrO_4 surface, much larger than other reported gap values.

The atomically resolved STM image obtained at the (661) facet (Fig. 3a) shows a nearly hexagonal lattice on this surface. The interatomic distance is about 3.7 Å, very close to the a -axis lattice constant of 3.78 Å. The exposed surface structure of (661) plane is composed of a mixture of Sr and Ir atoms located in same plane. The

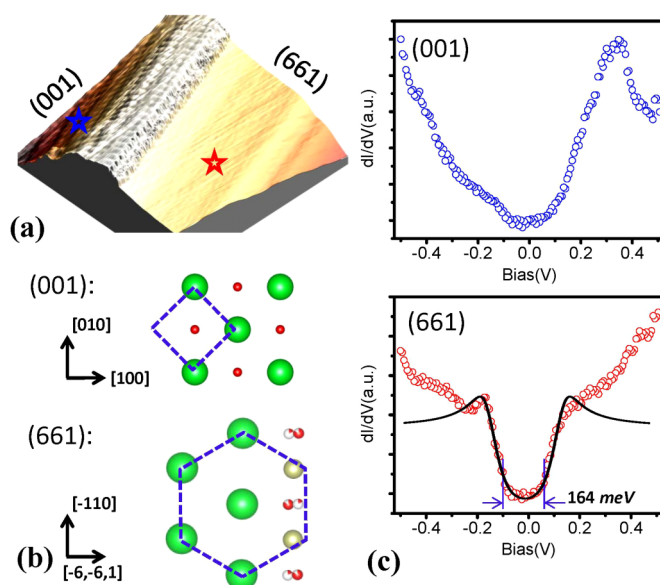


Figure 2 | Crystallographic planes with different orientations. (a), A 3D landscape of scan area, showing two differently orientated surfaces after cleaving. The left facet is the (001) plane, while the right facet is determined as (661) plane. (b), The ball models of surface atomic structures for (001) plane and (661) plane. The basic surface unit cells are marked by blue dashed lines. (c), Local tunneling spectra were taken on the locations within different planes marked as stars in panel (a), showing the variation of the insulating gap in different crystalline planes. The gap size can be estimated to be approximately 164 meV from the fitting of spectra. The fitting curves are shown as black lines in the same plots as the experimental STS data. All spectral surveys were taken with a sample-bias voltage of 20 mV, a tunneling current of 0.1 nA, and bias modulation amplitude of 3 mV_{rms}.

interatomic distance between Sr and Sr (green (color)) is 3.78 Å, while the Ir-Ir and Sr-Ir distances are smaller (about 3.36 Å). Such discrepancy gives rise to a slight distortion of the hexagonal lattice. The distortion is clearly illustrated by the Fourier transform (FFT) image shown in Fig. 3b, which further confirms the measured surface is the (661) plane (Fig. 2b).

To obtain further insight into the variability of electronic structure on (661) surface, a spectroscopic survey was taken on the region marked by the dashed, blue (color) square in Fig. 3a, which consists of a 40×40 differential tunneling conductance spectra (dI/dV vs. V) grid in the given region. This 3D data set provides a detailed spatial map of the local density of states (LDOS) as a function of energy E . Most dI/dV spectra acquired (in Fig. 3d) exhibit similar gap features, implying such insulating gap is intrinsic and homogeneous. Surprisingly, tunneling spectra at some locations (*e.g.* marked as a blue star in Fig. 3a) have two prominent peaks at the gap edges (Fig. 3c), strongly resembling quasi-particle coherence peaks found in tunneling spectrum for superconductors^{29,30}. Such spectra are expected for Slater insulators and are consistent with our DMFT calculations (see Fig. 4c). Such peak-gap features can be fitted by phenomenological AF mean-field theory by considering a Dynes broadening factor Γ ³¹, which is convoluted with the Fermi function at 4.2 K. This resulted in the fitting parameters $\Gamma = 20$ meV and $\Delta = 160$ meV. The fitted curve (red line in Fig. 3c) is in good agreement with the STS data shown by the dotted curve.

Discussion

In order to gain further insight into the origin of the ground state in Sr_2IrO_4 , we performed DFT calculations (details are given in the Methods section). With a realistic value (Ref. 11) of the parameter

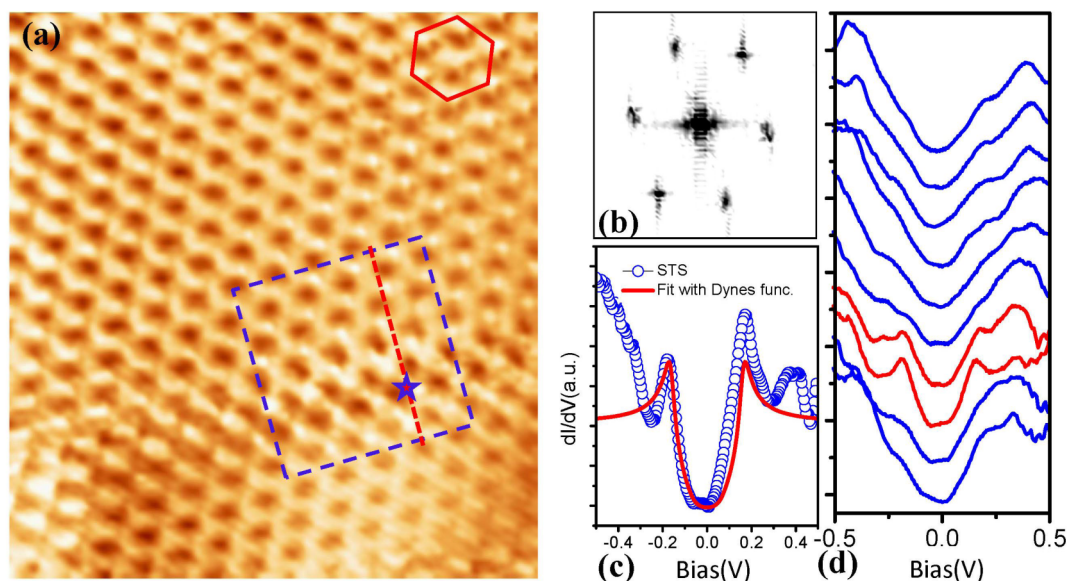


Figure 3 | Atomic structure and BCS-like gap on (661) surface. (a), Atomically resolved STM image on (661) surface, showing a distorted hexagonal atomic structure. Scan size is $5 \text{ nm} \times 5 \text{ nm}$. The image was taken at the bias of 50 mV with 100 pA tunneling current. (b), The FFT image displays a pseudo-hexagonal reciprocal lattice. (c), Point tunneling spectrum taken at the location marked as star in panel (a) shows a well-defined gap feature and two peaks at the gap edge. Such gap and peaks can be well fitted by phenomenological AF mean-field theory. The fitting details are described in support materials. (d), A series of spectra acquired along the red line in panel (a). The highlighted red curves have distinct peaks at the edge of the gap while the other curves do not.

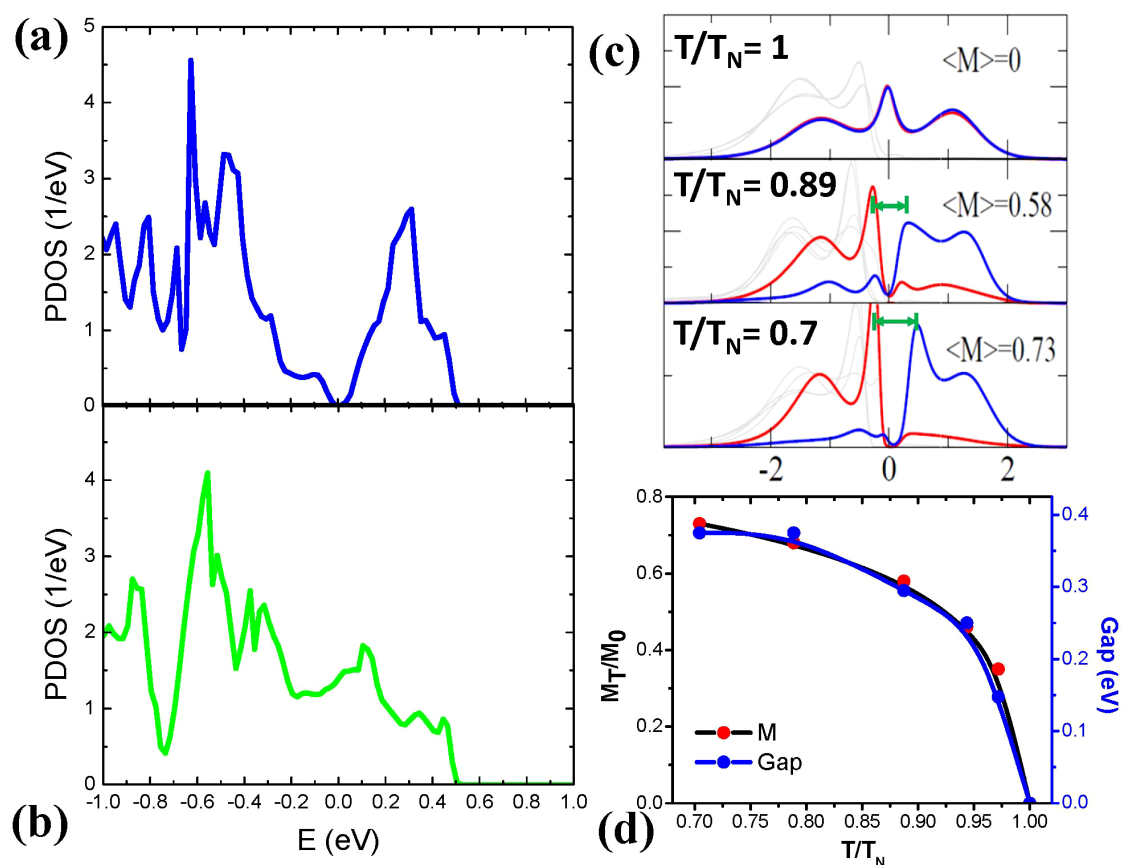


Figure 4 | Density of states, elevated temperature calculations of Sr_2IrO_4 . (a), LDA partial density of states of Sr_2IrO_4 projected onto Ir d states with consideration of AF ordering. (b), same as (a) but without AF ordering. (c), A series of PDOS projected onto $J_{\text{eff}} = 1/2$ and $3/2$ states of Ir obtained with LDA+DMFT for temperatures varying up to T_N . The blue and red lines are $|J_z\rangle = |1/2, 1/2\rangle$ and $|1/2, -1/2\rangle$, respectively and the grey lines are $J=3/2$ states. The gap value for temperature is estimated by the splitting between lower and upper Hubbard band as indicated. (d), Staggered magnetization M and the gap width as a function of temperature.

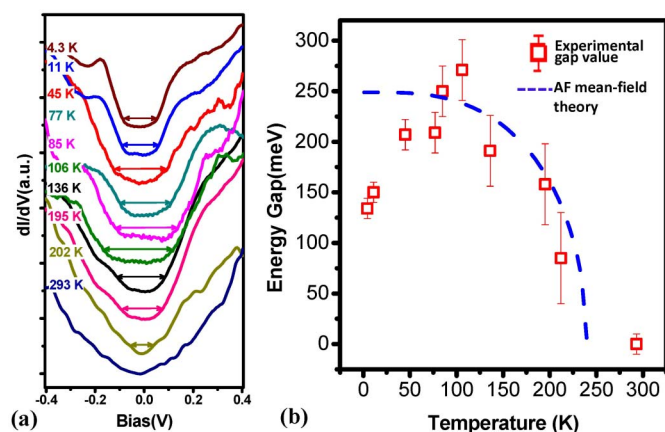


Figure 5 | Temperature dependence of the insulating gap measured by STS. (a), Temperature dependence of scanning tunneling dI/dV spectra measured at the surface of Sr_2IrO_4 (averaged over an area of $100 \text{ nm} \times 100 \text{ nm}$ by a grid spectroscopic mode with 20×20 sampling pixels, sample bias $V = -50 \text{ mV}$, and feedback current $I = 100 \text{ pA}$). The spectra are shifted for clarity. (b), Temperature dependence of the energy gap determined by the STS spectra. The blue dashed curve is the temperature dependence of the energy gap obtained by a phenomenological AF mean-field theory for comparison.

$U = 2.5 \text{ eV}$, the ground state is found to be a canted AF insulator, which is consistent with experimental results. The resulting projected density of states (PDOS) is presented in Fig. 4a (the corresponding band structure is consistent with a previous study⁷, and is shown in the SOM, Fig. S5). The spectral intensity near E_F is suppressed over a rather wide energy range of 200 meV. This suppression is consistent with the STS measurements. At reasonably high temperatures, the spectral shape is expected similar to the one shown in Fig. 4b, where the magnetic ordering is suppressed with finite U .

The distinction between the Slater transition and the Mott transition is rather subtle as, even in the Slater systems, local moments could exist above the magnetic transition temperature due to non-zero interactions. However, the Slater mechanism entails strong correlation between magnetic ordering and the opening of the insulating gap. In order to see such a correlation near T_{MIT} more clearly, we extended our previous DFT-DMFT calculations for Sr_2IrO_4 ¹¹. The resulting spectral functions are presented in Fig. 4c for various temperatures. While at high temperatures, we obtain metallic paramagnetic solutions, the system clearly undergoes a transition to the AF phase at the Néel temperature (T_N). Additionally, the gap amplitude is increased as temperature is further lowered and the staggered magnetization is increased. Fig. 4d compares the staggered magnetization M and the gap amplitude as a function of temperature. We note that we define the gap as half of the energy splitting between the upper Hubbard band (UHB) and lower Hubbard band (LHB), as the low-energy edge is hard to resolve. We emphasize that the gap amplitude follows the staggered magnetic moment. As shown below, this behavior resembles our experimental measurements and provides evidence that gap formation in Sr_2IrO_4 is correlated with magnetic order, as expected for a Slater mechanism.

Figure 5a shows the temperature dependent STS spectra in the temperature interval 4–300 K. The evolution of the gap with temperature provides critical information regarding the origin of the insulating state. It is noteworthy that a rigorous tip-conditioning procedure has been adopted in order to maintain a sharp and metallic tip during our experiments. Tip contamination affects the spectroscopic measurements and could lead to unusually large gap.

At each temperature, the gap value is obtained by averaging spectra from an area of $100 \text{ nm} \times 100 \text{ nm}$ by using a grid spectroscopic mode with 60×60 sampling pixels. To minimize the effect of sample

inhomogeneity, grid spectroscopic measurements at different temperatures were obtained at almost the same surface region, manually tracking the location by accounting for the thermal drift of the STM. The STS spectrum at room temperature displays no sign of an energy gap. An energy gap opens in the STS spectra below T_N (Fig. 5a), indicating the establishment of an insulating state at the surface.

To elucidate the correlation of these changes, we have analyzed the STS spectra to extract information about the T dependence of the energy gap (Fig. 5b). With temperature increasing from 4 K, the gap value first increases from 150 meV to 250 meV at 100 K, followed by a continuous drop to zero at room temperature. The error in the estimated gap size originates from the uncertainty in determining the gap feature when the temperature is near T_N (240 K). A gap function (blue dashed line) obtained from a phenomenological mean-field theory for the Slater AF is also plotted for comparison. The self-consistent equation for the AF mean-field theory is mathematically equivalent to the BCS gap equation. Thus, a Slater insulating gap will behave in much the same way as a BCS gap³². As is clear from Fig. 5b, the temperature dependence of the insulating gap of Sr_2IrO_4 is consistent with the Slater scenario at least for temperatures between about 100 and 240 K. Since STM/S is a surface-sensitive technique, it will be better to provide direct comparison of temperature dependences for both surface magnetic ordering and gap value. It will be a great interest to explore the surface antiferromagnetism of Sr_2IrO_4 by surface spin-sensitive techniques (such as spin-polarized STM, spin-polarized low energy electron diffraction, etc.) in future. Although surface magnetism may be different from the bulk due to broken symmetry at surface, our temperature-dependent gap measurement shows a similar trend as the bulk magnetism, thus suggest a similar magnetic behavior on the surface, which can be understood based on strong electronic and magnetic coupling between the surface layer and inner layers.

The discrepancy between the experimental (Fig. 5b) and theoretical (Fig. 4d) temperature dependences of the energy gap can be understood by considering the temperature dependence of the magnetization of Sr_2IrO_4 with a magnetic field applied along the a or c directions^{33,34}. According to a previous report³³, the easy axis is aligned in a direction and the canted AF order occurs around 240 K. In addition, the ac susceptibility starts to increase at around 50 K and reaches a peak at around 135 K, which is much lower than the magnetic transition temperature³³. This peak reflects a metamagnetic transition associated with a strong enhanced electric permittivity peak around 100 K. The increase of the dielectric constant near 100 K (about 1 order of magnitude) increases the effective bias voltage between the STM tip and the sample, as well as the measured energy gap. The similarities in the temperature dependences of the insulating gap and the reported magnetization of Sr_2IrO_4 ³³, strongly imply a magnetic origin for the insulating state, consistent with a Slater type transition.

It is interesting to note, however, that in STS we observe “U-shaped” spectra above T_N . As the thermal broadening is estimated to be about 100 meV ($4 k_B T$) at room temperature, such U-shaped spectra indicate the existence of a pseudogap, which is absent in single-site DFT-DMFT analyses (Fig. 4c). However, the evidence of a pseudogap is consistent with the optical conductivity³, which shows the closing of the gap without the Drude response, indicating a bad metal. Reference 17 reported the absence of the abrupt change in the resistivity around T_N . This is in fact consistent with the growth of the short-ranged antiferromagnetic correlation giving rise to the Anderson localization above T_N , making the temperature dependence of the resistivity rather smooth. While the Anderson localization hinders the detailed analyses, the resistivity anomaly can be visible by the Arrhenius plot across T_N ³⁵. As reported in Ref. 36, $d(\ln\rho)/d(T^{-1})$ indeed shows clear change around T_N , which is consistent with our picture. It remains an open question whether or not non-local effects can reproduce such pseudogap^{37–39} in Sr_2IrO_4 or



whether additional degrees of freedom are necessary, such as electron-phonon coupling⁴⁰, in Sr₂IrO₄. STM/S technique is a surface sensitive probe. Near the surface, correlation effects are expected to be stronger than in the bulk^{41,42} because of the smaller coordination number and concomitant suppressed screening. Interestingly, in contrast to Ca_{2-x}Sr_xRuO₄⁴³, the MIT in Sr₂IrO₄ does not involve a structural transition and the closing of the gap coincides with the bulk magnetic transition. Thus, Sr₂IrO₄ may be less strongly-correlated in the bulk.

In summary, we studied the metal-insulator transition and low temperature insulating state in Sr₂IrO₄ using STM/S techniques and found a BCS-like gap that opened smoothly as Sr₂IrO₄ was cooled below its Néel temperature. These results are most consistent with a Slater transition. Although the possibility of a Slater transition and the coexistence of Slater- and Mott-Hubbard-type behaviors have occasionally been discussed in the study of metal-insulator transitions in the iridates⁹, our tunneling spectroscopic results, combined with our DFT + DMFT theoretical studies, provide unambiguous evidence that instead of being driven only by *Coulomb interactions*, suggested by $J_{\text{eff}} = 1/2$ Mott-Hubbard model, the magnetic transition taking place at T_N points directly to the Slater-type origin of the insulating ground state of Sr₂IrO₄. The spectra further support an evolution of a strongly correlated metal above the Néel temperature characterized by the pseudogap formation.

Methods

Synthesis of Sr₂IrO₄ crystals. Single crystals of Sr₂IrO₄ were grown in Pt crucibles from a SrCl₂ flux using IrO₂, SrCO₃, and SrCl₂ as starting materials. The crucibles were heated to 1330 °C and held for 24 hours before slowly cooling at 2 °C/hour to 800 °C. At 800 °C the furnace was switched off and the crucible was allowed to cool to room temperature. The crystals grew as black plates with dimensions 1 × 1 × 0.2 mm³. The crystals were mechanically removed from the flux and characterized using microprobe analysis, X-ray diffraction, magnetization, and resistivity to confirm their physical properties were consistent with literature reports.

STM measurements. A laboratory-built low-temperature scanning tunneling microscope (STM) was used for the imaging and spectroscopic measurements. The sample was cleaved at room temperature in *ultra-high* vacuum (UHV) to expose a shining surface and then loaded into the STM head for investigation at various temperatures. We obtained topographic images in constant-current mode, and the tunneling spectra dI/dV using lock-in technique to measure differential conductance. A commercial Pt-Ir tip was prepared by gentle field emission at a clean Au(111) sample. The bias voltage was applied on the sample during the STM/S observations. The WSxM software has been used to process and analyze STM data⁴⁴.

DFT calculations. We performed the DFT calculations with the generalized gradient approximation (GGA) and projector augmented wave (PAW) approach⁴⁵ as implemented in the Vienna Ab initio Simulation Package (VASP)^{46,47}. The relativistic spin-orbit coupling is included. We used the experimental structure as provided in⁴⁸ with a $8 \times 8 \times 2$ k -point grid and an energy cutoff 550 eV, and the rotationally invariant LDA + U method of Liechtenstein *et al.*⁴⁹ with $U = 2.5$ and $J = 0.2$ eV for the Ir d states. The value of U is slightly larger than that estimated in Ref. 11. This is because the current value is for atomic d orbitals, while the estimation for U in Ref. 11 is for Wannier orbitals, thus additional screening effects are involved. For Ir and O, we used standard potentials (Ir and O in the VASP distribution), and for Sr, we used PAW potentials in which semicore s states are treated as valence states (Sr_{sv} in the VASP distribution). Details of DFT + DMFT calculations are provided in Ref. 11.

- Slater, J. C. Magnetic effects and the Hartree-Fock equation. *Phys. Rev.* **82**, 538–541 (1951).
- Moon, S. J. *et al.* Electronic structures of layered perovskite Sr₂MO₄ (M = Ru, Rh, and Ir). *Phys. Rev. B* **74**, 113104 (2006).
- Moon, S. J. *et al.* Temperature dependence of the electronic structure of the $J_{\text{eff}} = 1/2$ Mott insulator Sr₂IrO₄ studied by optical spectroscopy. *Phys. Rev. B* **80**, 195110 (2009).
- Crawford, M. K. *et al.* Structural and magnetic studies of Sr₂IrO₄. *Phys. Rev. B* **49**, 9198–9201 (1994).
- Kim, B. J. *et al.* Phase-sensitive observation of a spin-orbital Mott state in Sr₂IrO₄. *Science* **323**, 1329–1332 (2009).
- Martins, C., Aichhorn, M., Vaugier, L. & Biermann, S. Reduced effective spin-orbital degeneracy and spin-orbital ordering in paramagnetic transition-metal oxides: Sr₂IrO₄ versus Sr₂RhO₄. *Phys. Rev. Lett.* **107**, 266404 (2011).
- Kim, B. J. *et al.* Novel $J_{\text{eff}} = 1/2$ Mott state induced by relativistic spin-orbit coupling in Sr₂IrO₄. *Phys. Rev. Lett.* **101**, 076402 (2008).
- Haskel, D. *et al.* Pressure tuning of the spin-orbit coupled ground state in Sr₂IrO₄. *Phys. Rev. Lett.* **109**, 027204 (2012).
- Hsieh, D., Mahmood, F., Torchinsky, D. H., Cao, G. & Gedik, N. Observation of a metal-to-insulator transition with both Mott-Hubbard and Slater characteristics in Sr₂IrO₄ from time-resolved photocarrier dynamics. *Phys. Rev. B* **86**, 035128 (2012).
- Ye, F. *et al.* Magnetic and crystal structures of Sr₂IrO₄: A neutron diffraction study. *Phys. Rev. B* **87**, 140406(R) (2013).
- Arita, R., Kunes, J., Kozhevnikov, A. V., Eguluz, A. G. & Imada, M. *Ab initio* studies on the interplay between spin-orbit interaction and Coulomb correlation in Sr₂IrO₄ and Ba₂IrO₄. *Phys. Rev. Lett.* **108**, 086403 (2012).
- Calder, S. *et al.* Magnetically driven metal-insulator transition in NaOsO₃. *Phys. Rev. Lett.* **108**, 257209 (2012).
- Hu, B. *et al.* Surface and bulk structural properties of single-crystalline Sr₃Ru₂O₇. *Phys. Rev. B* **81**, 184104 (2010).
- Matzdorf, R. *et al.* Ferromagnetism stabilized by lattice distortion at the surface of the p -wave superconductor Sr₂RuO₄. *Science* **289**, 746–748 (2000).
- Moore, R. G. *et al.* A surface-tailored, purely electronic, Mott metal-to-insulator transition. *Science* **318**, 615–619 (2007).
- Iwaya, K. *et al.* Local tunneling spectroscopy across a metamagnetic critical point in the bilayer ruthenate Sr₃Ru₂O₇. *Phys. Rev. Lett.* **99**, 057208 (2007).
- Cao, G., Bolivar, J., McCall, S., Crow, J. E. & Guertin, R. P. Weak ferromagnetism, metal-to-nonmetal transition, and negative differential resistivity in single-crystal Sr₂IrO₄. *Phys. Rev. B* **57**, R11039–R11042 (1998).
- Fischer, Ø., Kugler, M., Maggio-Aprile, I. & Berthod, C. Scanning tunneling spectroscopy of high-temperature superconductors. *Rev. Mod. Phys.* **79**, 353 (2007).
- Hoffman, J. E. A search for alternative electronic order in the high temperature superconductor Bi₂Sr₂CaCu₂O_{8+δ} by scanning tunneling microscopy. Retrieved August 9, 2013, from <http://users.physics.harvard.edu/~jhoffman/thesis>.
- Hasegawa, T., Nantoh, M., Motohira, N., Kishio, K. & Kitazawa, K. Anisotropic electronic-structures in cuprate superconductors investigated by STM STS. *Supercond. Sci. Technol.* **4**, S73–S75 (1991).
- Suzuki, M., Watanabe, T. & Matsuda, A. Interlayer tunneling spectroscopy for slightly overdoped Bi₂Sr₂CaCu₂O_{8+δ}. *Phys. Rev. Lett.* **82**, 5361–5364 (1999).
- Kane, J. & Ng, K. W. Angular dependence of the in-plane energy gap of Bi₂Sr₂CaCu₂O₈ by tunneling spectroscopy. *Phys. Rev. B* **53**, 2819–2826 (1996).
- Yeh, N. C. *et al.* Evidence of doping-dependent pairing symmetry in cuprate superconductors. *Phys. Rev. Lett.* **87**, 087003 (2001).
- Hasegawa, T. & Kitazawa, K. Atomically resolved STM/STS observation on the edge of CuO₂ and (BiO)₂ Layers of Bi-Sr-Ca-Cu-O. *Jpn. J. Appl. Phys.* **29**, L434–L437 (1990).
- Nantoh, M. *et al.* Cryogenic scanning tunneling microscopy/spectroscopy on the (110) surfaces of YBa₂Cu₃O₇ epitaxial thin-films. *Physica C* **242**, 277–282 (1995).
- Watanabe, H., Shirakawa, T. & Yunoki, S. Microscopic study of a spin-orbit-induced Mott insulator in Ir oxides. *Phys. Rev. Lett.* **105**, 216410 (2010).
- Nichols, J., Bray-Ali, N., Cao, G. & Ng, K. W. Direct observation of the Mott gap in strontium iridate with a scanning tunneling microscope. *arXiv:1302.5431* (2013).
- Dai, J. X., Calleja, E., Cao, G. & McElroy, K. Local density of states study of a spin-orbit-coupling induced Mott insulator Sr₂IrO₄. *arXiv:1303.3688* (2013).
- Schrieffer, J. R., Scalapino, D. J. & Wilkins, J. W. Effective tunneling density of states in superconductors. *Phys. Rev. Lett.* **10**, 336–339 (1963).
- Rowell, J. M., Anderson, P. W. & Thomas, D. E. Image of the phonon spectrum in the tunneling characteristic between superconductors. *Phys. Rev. Lett.* **10**, 334–336 (1963).
- Dynes, R. C., Narayanamurti, V. & Garno, J. P. Direct measurement of quasiparticle-lifetime broadening in a strong-coupled superconductor. *Phys. Rev. Lett.* **41**, 1509–1512 (1978).
- Matsubara, T. & Yokota, Y. In *Proceedings of the International Conference on Theoretical Physics, Kyoto-Tokyo*, (Sci. Council Japan, Tokyo, 1954), p. 693 (1953).
- Chikara, S. *et al.* Giant magnetoelectric effect in the $J_{\text{eff}} = 1/2$ Mott insulator Sr₂IrO₄. *Phys. Rev. B* **80**, R140407 (2009).
- Calder, S. *et al.* Magnetic structural change of Sr₂IrO₄ upon Mn doping. *Phys. Rev. B* **86**, R220403 (2012).
- Nichols, J. *et al.* Anisotropic electronic properties of a-axis-oriented Sr₂IrO₄ epitaxial thin-films. *arXiv:1308.4221*.
- Kini, N. S., Strydom, A. M., Jeevan, H. S., Geibel, C. & Ramakrishnan, S. Transport and thermal properties of weakly ferromagnetic Sr₂IrO₄. *J. Phys. Condens. Matter* **18**, 8205 (2006).
- Huscroft, C., Jarrell, M., Maier, Th., Moukouri, S. & Tahvildarzadeh, A. N. Pseudogaps in the 2D Hubbard model. *Phys. Rev. Lett.* **86**, 139–142 (2001).
- Kyung, B. *et al.* Pseudogap induced by short-range spin correlations in a doped Mott insulator. *Phys. Rev. B* **73**, 165114 (2006).
- Zhang, Y. Z. & Imada, M. Pseudogap and Mott transition studied by cellular dynamical mean-field theory. *Phys. Rev. B* **76**, 045108 (2007).
- Millis, A. J., Mueller, R. & Shraiman, B. I. Fermi-liquid-to-polaron crossover. I. General results. *Phys. Rev. B* **54**, 5389–5404 (1996).
- Liebsch, A. Surface versus bulk coulomb correlations in photoemission spectra of SrVO₃ and CaVO₃. *Phys. Rev. Lett.* **90**, 096401 (2003).
- Eguchi, R. *et al.* Bulk- and surface-sensitive high-resolution photoemission study of two Mott-Hubbard systems: SrVO₃ and CaVO₃. *Phys. Rev. Lett.* **96**, 076402 (2006).



43. Moore, R. G. *et al.* Manifestations of broken symmetry: The surface phases of $\text{Ca}_{2-x}\text{Sr}_x\text{RuO}_4$. *Phys. Rev. Lett.* **100**, 066102 (2008).
44. Horcas, I. *et al.* WSXM: A software for scanning probe microscopy and a tool for nanotechnology. *Rev. Sci. Instrum.* **78**, 013705 (2007).
45. Blochl, P. E. Projector augmented-wave method. *Phys. Rev. B* **50**, 17953 (1994).
46. Kresse, G. & Furthmüller, J. Efficient iterative schemes for *ab initio* total-energy calculations using a plane-wave basis set. *Phys. Rev. B* **54**, 11169 (1996).
47. Kresse, G. & Joubert, D. From ultrasoft pseudopotentials to the projector augmented-wave method. *Phys. Rev. B* **59**, 1758 (1999).
48. Rowell, J. M., Anderson, P. W. & Thomas, D. E. *Phys. Rev. Lett.* **10**, 334 (1963).
49. Liechtenstein, A. I., Anisimov, V. I. & Zaanen, Z. Image of the phonon spectrum in the tunneling characteristic between superconductors. *Phys. Rev. B* **52**, R5467 (1995).

Acknowledgements

This research was conducted (MP, QL, ZG) at the Center for Nanophase Materials Sciences, which is sponsored at Oak Ridge National Laboratory by the Scientific User Facilities Division, Office of Basic Energy Sciences, U.S. Department of Energy. Research was supported (GXC, SO, WL, JYY, BCS, JQY, DGM) by the U.S. Department of Energy, Basic Energy Sciences, Materials Sciences and Engineering Division. RA and MI were supported by MEXT Japan and Strategic Programs for Innovative Research (SPIRE), MEXT, and the Computational Materials Science Initiative (CMSI), Japan. JK was supported by the Grant No. 13-25251S of the Grant Agency of the Czech Republic. AVK acknowledges the

computational resources of the CSCS and of the NCCS and the CNMS at ORNL, which are sponsored by the respective facilities divisions of the offices of ASCR and BES of the U.S. DOE. AGE was supported by NSF Grant No. OCI-0904972.

Author contributions

Q.L., W.L., M.P. performed STM measurements and analyzed STM data. G.X.C., J.Q.Y., B.C.S., D.G.M. grew and characterized the crystals. J.Y.Y., Z.G. performed the LEED measurements. S.O., R.A., J.K., A.V.K., A.G.E., M.I. carried out theoretical calculations. All authors discussed the results and M.P. wrote the paper with help from all authors. We thank Sergei V. Kalinin for careful reading.

Additional information

Supplementary information accompanies this paper at <http://www.nature.com/scientificreports>

Competing financial interests: The authors declare no competing financial interests.

How to cite this article: Li, Q. *et al.* Atomically resolved spectroscopic study of Sr_2IrO_4 : Experiment and theory. *Sci. Rep.* **3**, 3073; DOI:10.1038/srep03073 (2013).



This work is licensed under a Creative Commons Attribution-NonCommercial-NoDerivs 3.0 Unported license. To view a copy of this license, visit <http://creativecommons.org/licenses/by-nc-nd/3.0>